Tunable Far-IR Detectors/Filters Based on Plasmons in Two Dimensional Electron Gases in InGaAs/InP Heterostructures

W. R. Buchwald[a], H. Saxena[b], R. E. Peale[b]
[a]Air Force Research Laboratory, Sensors Directorate, Hanscom AFB MA 01731
[b]University of Central Florida, Physics Department, Orlando FL 32816

ABSTRACT

Plasmons can be generated with photons in the two dimensional electron gas (2-deg) of high electron mobility transistors (HEMTs). Because the plasmon frequency at a given wavevector depends on sheet charge density, a gate bias can tune the plasmon resonance. This effect allows a properly designed HEMT to be used as a voltage-tunable narrow-band detector or filter. This work reports on both the theory and design of such a device in the InP materials system and discusses its potential uses. By using a sub-micron grating to couple incident radiation to a high sheet charge 2-deg, a minimum detectible wavelength of roughly 26 microns is obtained. Fabrication issues, terahertz response, and tunability are discussed. Because of its small size, this novel device could find use in spaceborne remote sensing application.

Keywords: Plasmon, terahertz, 2-deg, HEMT

1. INTRODUCTION

Plasmons are charge density oscillations whose generation in semiconductor heterostructures provides a mechanism for tunable wavelength-selective detection at terahertz frequencies. This class of frequency agile detector holds promise for the development of a true spectrometer-on-a-chip for chemical and biological detection due to the rich spectra found at these frequencies. Two-dimensional plasmon resonances observed in Si MOSFETs[1] and AlGaAs-based semiconductor heterostructures[2,3] tune with 2-deg sheet charge density, which is controlled by a gate bias. Surprisingly, a change in device conductivity has also been found to accompany the plasmon resonance of such devices. This has led to research concerning the use of high electron mobility transistors (HEMT's) as frequency agile, voltage tunable detectors. In effect, incident THz radiation excites a bias-controlled plasmon resonance, which is observed as a change in the device transconductance. This work explores a device design based on the InP materials system, which is new. We report on maximum achievable resonance frequency, tuning range, resonance linewidth, temperature effects, incident radiation coupling considerations, and device fabrication.

2. BACKGROUND

The dispersion relationship for a plasmon in a 2-deg is[1]

$$\omega_p(k_p) = \sqrt{\frac{n_s q^2 k_p}{m^* \varepsilon_o(\varepsilon_b + \varepsilon_t Coth(k_p d))}} \quad , \tag{1}$$

where all quantities are expressed in S.I. units, ω_p is the plasmon frequency, k_p is the plasmon wave vector, q is the elementary charge, m^* is the electron effective mass in the 2-deg, d is the distance of the 2-deg below the semiconductor surface, ε_b and ε_t are the relative dielectric constants of the material below and above the 2-deg respectively, ε_0 is the permittivity of free space, and n_s is the 2-deg sheet charge density. Eq. (1) shows that for any incident photon with wave vector $k_i (=\frac{\omega_i}{c})$ and any angle of incidence, photon momentum is insufficient to excite a plasmon, i.e for $\omega_i = \omega_p, k_{i\|} < k_p$ always. To conserve momentum and excite a plasmon, additional in-plane photon momentum can be acquired from a grating on the semiconductor surface. For normal incidence, the acquired parallel component of the wavevector is

$$G_m = 2\,\pi\, m/a \,, \tag{2}$$

where a is the grating period, and m is an integer (m= ± 1,2,…). Thus, for radiation at normal incidence to a properly designed grating, both energy and momentum can be conserved in the generation of a plasmon with $G_m = k_p$. The grating (possibly enhanced by an underlying semitransparent metallic layer) can also serve as the transistor gate to permit bias-control of the 2-deg sheet charge density (n_s) and tuning of the resonance frequency, thereby creating a spectrometer-on-a-chip.

3. DEVICE DESIGN

The detection range of this type of detector is determined by the sheet charge density, electron effective mass in the 2-deg, and the grating period. Because larger grating periods are easier to fabricate, and because lower sheet charge densities are easier to obtain, this type of device is best suited to long wavelengths. A goal of this work is to seek shorter wavelength response than has been achieved previously. The epitaxial layer structure presented schematically in Fig. 1 is chosen because similar InGaAs/InAlAs/InP structures have demonstrated high sheet charge densities.[4,5]

Eqs. (1) and (2) determine the high frequency limit of the Fig. 1 structure. Required material parameters are found as follows. The permittivity of semiconductor alloy $A_{1-x}B_x$ is determined from the permittivities ε_A, ε_B of the end members A,B according to

$$\varepsilon_{AB} = (1-x)\varepsilon_A + x\varepsilon_B - x(1-x) \quad , \tag{3}$$

for both InGaAs and InAlAs.[6] Using ε_{AlAs}=10.2, ε_{InAs}=14.6, and ε_{GaAs}=13.1, we obtain ε_t=12.2 for the $In_{0.52}Al_{0.48}As$ layer above the 2-deg and ε_b=13.9 for the $In_{0.68}Ga_{0.32}As$ below the 2-deg. Using an effective mass of 0.043 for electrons in the InGaAs channel,[7] we obtain from Eq. (1) a plot (Fig. 2) of excitation frequency versus sheet charge density and grating period. From Fig. 2, a grating period of 0.1 μm and a sheet charge density of 3 x 10^{12} cm^{-2} provide a minimum detectible wavelength of 26 μm.

75A $In_{0.60}$ $Ga_{0.40}As$ 6x10^{18} cm^{-3} Cap
350A $In_{0.52}$ $Al_{0.48}As$ Buffer Undoped
4x10^{12} cm^{-2} Si δ doping
30A $In_{0.52}$ $Al_{0.48}As$ Set Back Undoped
200A $In_{0.68}$ $Ga_{0.32}As$ Channel
30A $In_{0.52}$ $Al_{0.48}As$ Set Back Undoped
4x10^{12} cm^{-2} Si δ doping
3000A $In_{0.52}$ $Al_{0.48}As$ Buffer Undoped
Semi-insulating InP substrate

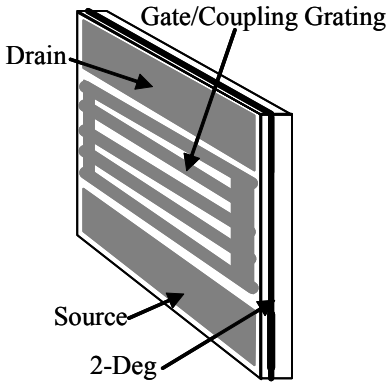

Fig. 1. Epi-layer structure and device schematic used for the voltage tunable plasmon based detector of this work

To determine the effects of gate bias, the 2-deg sheet charge density, n_s, is given by

$$n_S = C_{gate}\frac{(V_g - V_t)}{qLW}, \tag{4}$$

where V_g is the gate bias, V_t is the device threshold voltage, L is the gate source to drain spacing, W is the gate width and C_{gate} is the gate capacitance. The latter can be approximated (in S.I. units) by

$$C_{gate} = \frac{\varepsilon_t \varepsilon_o LW}{d} \quad . \tag{5}$$

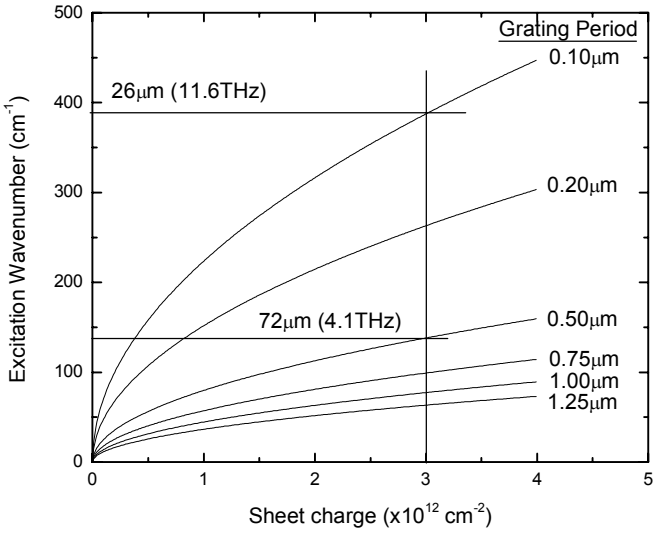

Fig. 2. Incident excitation wave number as a function of 2-deg sheet charge density for various grating periods.

The threshold voltage, V_t, is given by

$$V_t = \phi_b - E_c - \frac{qn_d d}{\varepsilon_t}, \tag{6}$$

where n_d is the delta doping concentration of the heterostructure and E_c is the conduction band offset. For the InGaAs/InAlAs system, when the In mole fraction in $In_xGa_{1-x}As$ exceeds 58%, E_c is given by [8]

$$E_c = 0.344 + 0.487x \quad . \tag{7}$$

For an MBE grown epi-layer structure of Fig. 1 design, Hall measurements indicate a sheet charge density of 2.4 x 10^{12} cm^{-2} and a mobility of 10100 (26500) cm^2/V-s at 300 (77) K. Using a typical barrier height for metal on a III-V compound of ϕ_b = 0.7 eV and all other values as previously defined, a linear decrease in sheet charge is expected with a maximum value at V_g=0 and zero at V_g=-1.3 V.

Fig. 3 presents the physical layout of the device studied theoretically in this work and to be explored experimentally in the near future. The overall chip size is 3.5 mm x 3.5 mm with the gate/grating measuring 250 μm x 195 μm. Care was taken to overlap all of the various metallization layers so that light can only be transmitted through the central gate/grating region of the device. The gate/grating section of this device is fabricated by first depositing a semitransparent Ti layer (with a sheet resistance assumed for calculation purposes to be $\rho_h \sim 350\Omega/sq.$) On top of this will be deposited Au grating stripes (with a sheet resistance assumed for calculations to be $\rho_l \sim 0.14\Omega/sq.$) Initial measurements on this device will be made using a high-power THz p-Ge laser at liquid helium temperatures. A multimode output spectrum presented in figure 4a demonstrates its suitable bandwidth[9] and a range of features that can be recorded as the device resonance tunes with gate bias. The device of Figure 3 is mounted in the He dewar between the p-Ge laser and a Ge:Ga photodetector as shown in Figure 4b. Electrical leads connecting source, drain and the gate/grating are then used to vary the sheet charge density while monitoring the device transconductance. Transmission through the device can be simultaneously monitored with the 4 K Ge:Ga photoconductor. Based on the spectrum for the

p-Ge laser and the maximum measured sheet charge of the epilayers, a grating period of 0.5 μm has been chosen to allow tunable detection across the entire output bandwidth of the laser with gate voltages from 0 V to -0.6 V.

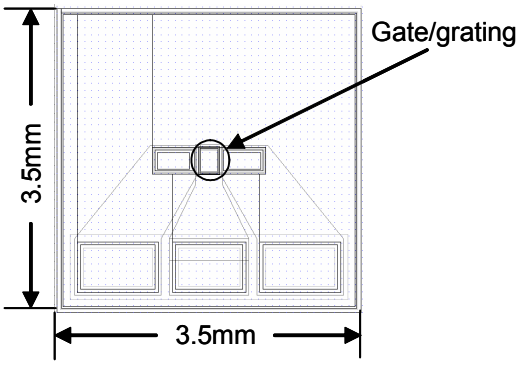

Fig. 3. Physical layout of device used in this work. Overlapping metal ensures light only passes through central gating/gate for maximum dynamic range during transmission measurements.

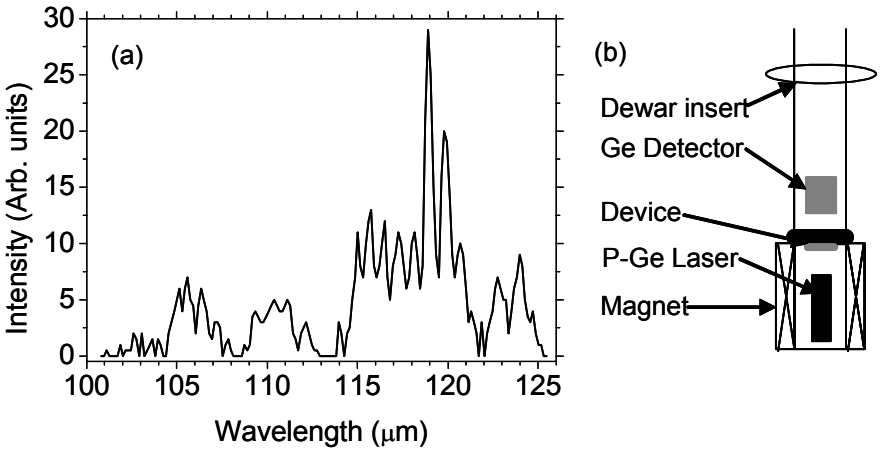

Fig. 4. (a) Typical output spectra of p-Ge laser used to excite plasmon resonance and (b) Schematic of transmission and photoconductivity experiment.

4. CALCULATIONS

To determine the features of the Plasmon resonance spectra in more detail, the theory of plasmons in grating-coupled 2-deg devices is used here.[10] Referring to Fig. 5, spatially uniform THz electric fields polarize the grating bars, which induces local fringing fields with the grating periodicity. These *x*-*y* polarized local fringing fields excite the plasmons in the 2-deg. The transmittance, *T*, of un-polarized light is

$$T=(T_y+T_z)/2 \ , \tag{8}$$

where T_y in zero magnetic field and in Gaussian units is

$$T_y = \sqrt{\varepsilon_b}\left|\frac{2}{1+\sqrt{\varepsilon_b}+\Sigma_{yy}\frac{4\pi}{c}}\right|^2 , \tag{9}$$

and T_z is obtained by substituting z for the y subscript. The complex yy-component of the conductivity tensor is

$$\Sigma_{yy} = \sigma(\omega) + \sigma^g_{yy} , \tag{10}$$

while the zz-component is given by

$$\Sigma_{zz} = \sigma(\omega) + <\sigma^g_{zz}> , \tag{11}$$

where < > indicates a spatial average, and $\sigma(\omega)$ is the conductivity associated with the 2-deg only. The second terms are components of the grating conductivity tensor. Only σ_{yy}^g interacts with the 2-deg. The $<\sigma_{zz}^g>$ is independent of the 2-deg because of the lack of fringing field components polarized in the z-direction. All off-diagonal components of Σ vanish in the absence of a magnetic field.

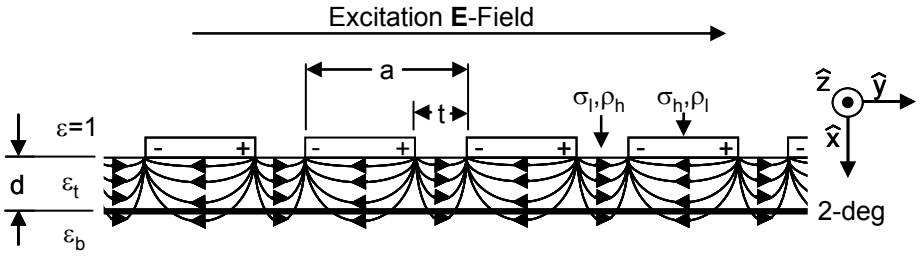

Fig. 5. Illustration of effects of incident excitation field on grating and in-turn on the 2-deg for this device.

The frequency dependent conductivity of the 2-deg is

$$\sigma(\omega) = \frac{n_s q^2 \tau}{m^*(1+\omega^2\tau^2)} , \tag{12}$$

where τ ($=\frac{m^*\mu}{q}$) is the electron relaxation time and μ is the temperature-dependant electron mobility. The last term of Eq. (10) is treated in the perturbative approximation according to

$$\sigma^g_{yy} = \frac{1}{<\rho>} - \sum_{m>0}\left(\frac{\tilde{\rho}(m)}{<\rho>}\right)^2 \frac{F_m}{2} , \tag{13}$$

where $<\rho>$ is the spatially averaged 2D resistivity of the grating, $\tilde{\rho}(m)$ is the m^{th} Fourier coefficient in the Cosine expansion of the yy-component for the grating resistivity tensor given by

$$\tilde{\rho}(m) = \frac{2}{\pi m}(\rho_h - \rho_l)\,Sin\frac{\pi t m}{a} , \tag{14}$$

and

$$F_m = (i\omega/4\pi G_m)\left[1+\varepsilon_t Coth(G_m d)+\frac{\varepsilon_b^2\,(1-Coth^2(G_m d))}{\frac{4\pi i}{\omega}G_m\sigma(\omega)+\varepsilon_b+\varepsilon_t Coth(G_m d)}\right]. \quad (15)$$

Following Ref. 10, the sum Eq. (13) is truncated after m = 10.

For the Fig. 1-based as grown MBE structure, electron relaxation times of τ = 0.25 (0.65) ps were measured at 300 (77) K. As will be shown below, these values are insufficiently high to produce sharp plasmon resonances, but they can be increased by cooling the device. Fig. 6 plots τ vs T, where the measured data points appear as symbols. Assuming that phonon scattering dominates the carrier relaxation, the temperature dependence should obey a power law with a -3/2 exponent,[11] which we use to estimate the low temperature τ values even though the actual data fall on a curve with an exponent closer to -0.70 (light line).

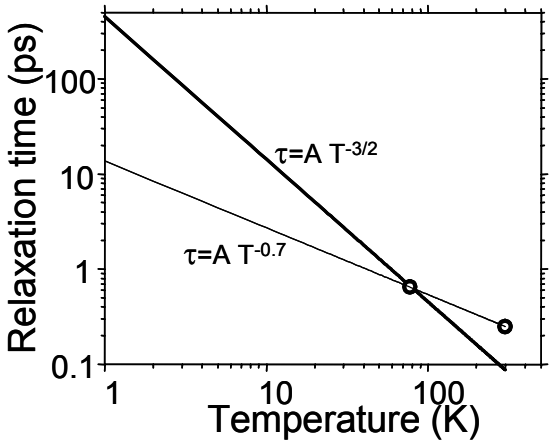

Fig. 6. Temperature dependence of the relaxation times for the 2-deg of this work. Symbols represent values calculated from the measured mobility. The $T^{-3/2}$ curve (heavy line) is a least squares fit to the data and was used for all simulations, although the $T^{-0.7}$ curve (light line) represents a better fit to the limited data.

Based on the theory and design presented above, transmission spectra are calculated, assuming a grating period a = 0.5 μm and a 2-deg depth d = 37 nm. Fig. 7 illustrates the effects of sheet charge and effective mass uncertainty at 4 K, where the sheet charge density of 2.4 x 10^{12} cm^{-1} is varied by a factor of two, while the effective mass of 0.043 is increased by 50% to 0.065.[12] With these changes in material parameters no change is seen in the plasmon FWHM of ~1.0 cm^{-1}. Changing the effective mass by 50% however causes a 19% decrease in the peak position wave number. Changing only the sheet change by a factor of two causes a 29% decrease in the peak position wave number. Uncertainty in peak position of this magnitude does not affect our planned experiment with the p-Ge laser, whose full tuning range is 50-140 cm^{-1}. It is noted, that although the peak position accompanying these material changes could be determined by the much simpler Eq. (1), the more detailed theory of Ref [10] is required to determine the overall plasmon line shape.

Resonance line width and absorption strength depend on temperature as shown in Figure 8 (a) and (b). Figure 8 (a) shows typical 1st order transmittance spectra for n_s = 2.4 x 10^{12} cm^{-2} and t/a = 0.65. The temperature dependence of metallization resisitivity is ignored because resistivity changes in the semi-transparent gate affect mainly the baseline transmittance. Moreover, residual resistance for thin semitransparent Ti films can be so high that the temperature dependance is weak.[13] The thick Au grating bars are opaque and the decrease in their resistivity with cooling has no effect on the spectrum at all. Fig. 8 (a) shows that there is still a small but measurable signal even at a temperature of 100 K. Figure 8 (b) plots both the percentage change of the transmittance as well as the simulated full width half maximum (FWHM) of the resonance peak for both 1st and 2nd order resonances. It is clear from this plot that the 2nd order peaks are not as deep and are slightly narrower in line width at lower temperatures.

Figure 9 presents the transmission plotted as a function of t/a ratio for both the 1st and 2nd order resonances. Figure 9 (a) shows similar peak heights for all *t/a* ratios with a slight narrowing of the peak as the *t/a* ratio is increased. Figure 9 (b) shows a rapid reduction in peak height as the *t/a* approaches the symmetric case of *t/a* = 0.5. This is caused by the impossibility of even-order terms occurring in the Fourier expansion of the fringing fields when the grating is symmetric (Fig. 5).

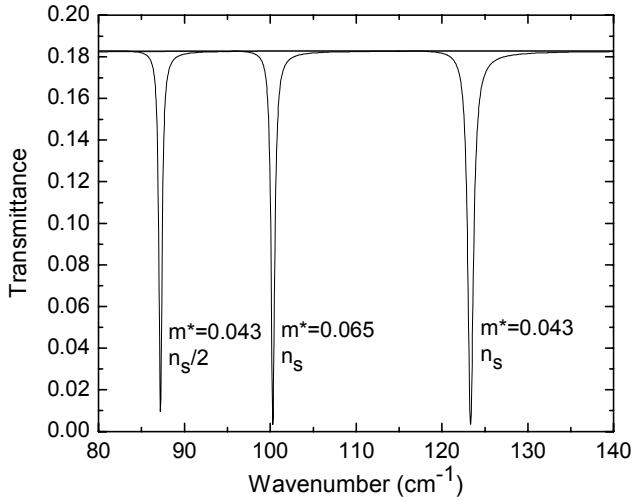

Fig. 7. Simulated transmittance for the device of this work showing effects of changes to effective mass and 2-deg sheet charge density.

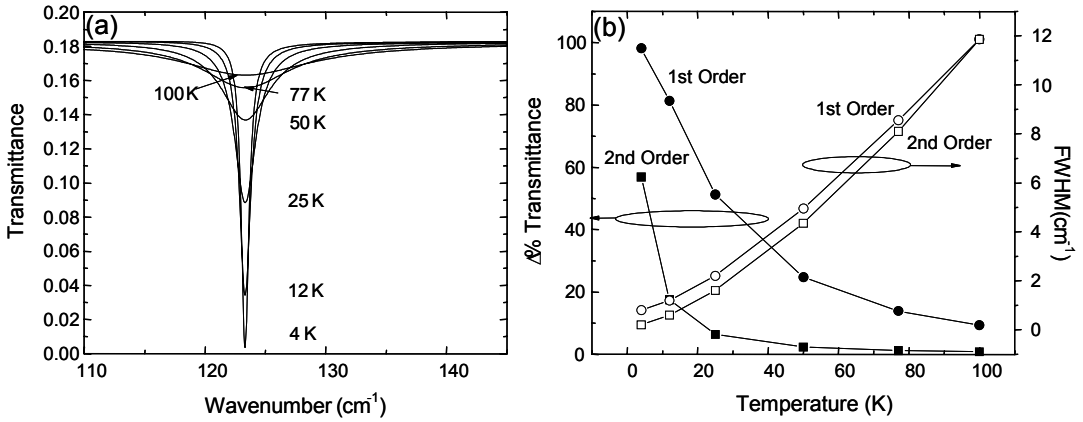

Fig. 8(a). Simulated transmittance showing effects of temperature on both percent change in transmittance and linewidth. (b) Details of similar measurements for both first and second order plasmon resonances.

5. DISCUSSION

The calculated spectra suggest that plasmon resonances can be generated from incident radiation having a short wavelength limit of roughly 26 μm. These resonances will alter the transmission through the device producing a voltage variable band-blocking filter of FWHM less than 1 cm^{-1} at 4K and 5 cm^{-1} at 50 K. Alternatively, because plasmons influence the 2-deg channel conductance, the device can be operated as a frequency-selective photo-conducting transducer. Fig. 10 illustrates the calculated voltage tunability where device transmittance is plotted at various gate biases. For this and all subsequent figures a *t/a* ratio of 0.65 and a zero bias 2-deg sheet charge of 2.4 x 10^{12} cm^{-2} are used. As can be seen, a voltage swing of 0.55 volts allows for detection of incident radiation from roughly 2.75 THz to

3.75 THz. In principle, increasing the grating period can shift this 1 THz detection band for the given semiconductor layer structure to any desired lower frequency.

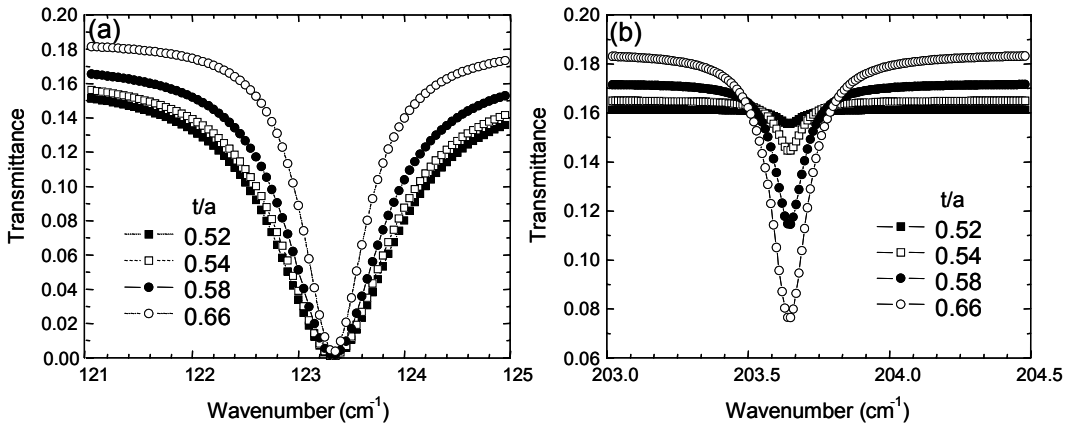

Fig. 9. Calculated effect of changing grating duty *t/a* on the (a) first order and (b) second order plasmon induced transmission spectrum.

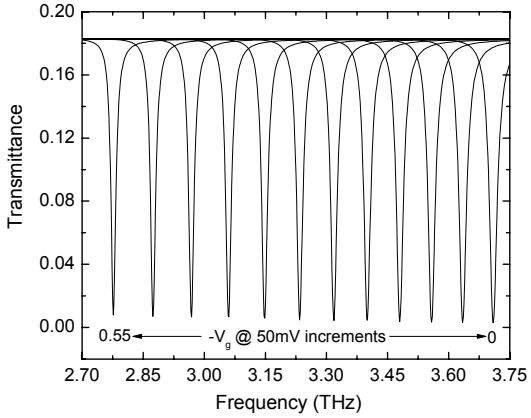

Fig. 10. Resonance tuning with gate voltage.

Two modes of operation for spectroscopy with the considered device can be envisioned. As a voltage tunable band-blocking filter before a broad band detector, it can be useful for spectroscopy of narrow-band molecular emission. In this mode, the detector output Γ is proportional to the product of the incident spectral density $I(\omega)$ and filter transmittance T, integrated over the detector bandwidth

$$\Gamma(\omega, V_g) = \int I(\omega) T(\omega, V_g) d\omega \ . \quad (16)$$

Figure 11 (a) is a simulated emission spectrum with two resonance peaks separated by 4 cm^{-1}, with each peak having a FWHM of 0.4 cm^{-1}. Figure 11 (b) shows a simulation of the detector response as a function of temperature and illustrates how the increased FWHM of the device transmittance at elevated temperatures effects overall spectral resolution. It is interesting to note, that even a 4 cm^{-1} peak separation can still be resolved at a temperature as high as 50 K, which is in range of compact closed cycle Stirling refrigerators. A drawback of this mode of spectroscopy is that radiation blocked by the filter but within the detector bandwidth adds noise and reduces dynamic range. This effect can be minimized through the use of a prefilter to limit the spectral response to a narrow band.

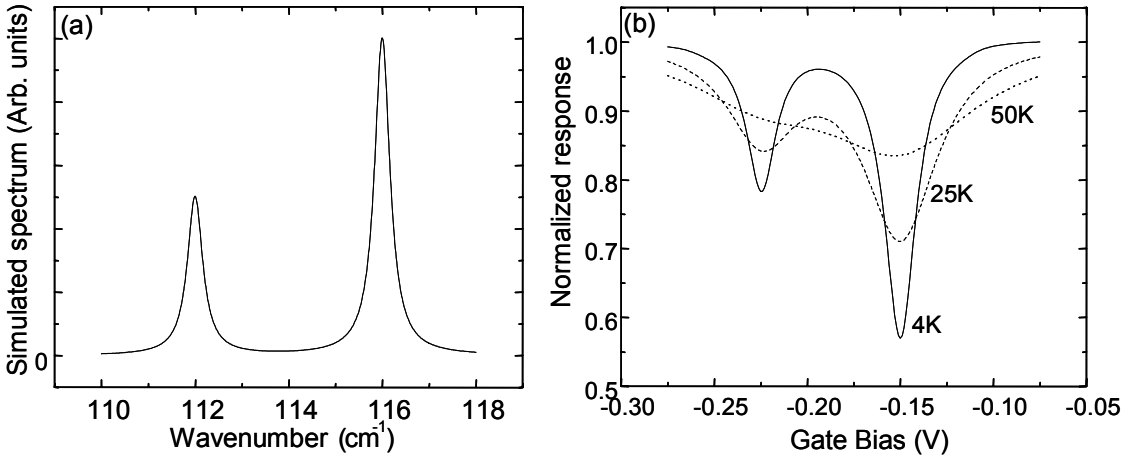

Fig 11 (a) Simulated incident radiation spectrum used to simulate (b) response of detector when the device of this work is used as a tunable notch filter.

A potentially cleaner mode of operation is as a voltage tunable detector where absorbed radiation within the plasmon resonance is sensed as a change in the source/drain current of the device. Though this effect has been observed in the AlGaAs materials system,[2,3] this mode is still somewhat speculative because the mechanism of Plasmon-conductance interaction is unknown, and the sign, linearity, temperature dependence, and magnitude of the response all remain uncertain. These questions will be investigated experimentally.

6. CONCLUSION

Design issues related to a detector based on plasmon generation in a 2-deg have been reported. This device utilizes grating coupling of incident radiation to plasmon modes in the 2-deg of a heterostructure. These induced plasmon excitations cause changes to the device absorption properties as well as changes in current along the 2-deg. Two modes of operation are capable of determining the spectral content of THz radiation over a 1 THz bandwidth. The central frequency of operation is determined by the period of the grating coupler and the 2-deg sheet charge density. In one case the device is operated as a voltage tunable band-blocking filter, which would require a band-pass prefilter to optimize the dynamic range. In the second case, changes in device conductance caused by plasmon excitation determine the spectral content of incident radiation. Although device performance is optimized at liquid helium temperatures, simulations suggest that a 4 cm^{-1} spectral resolution is attainable at temperatures as high as 50 K.

7. ACKNOWLEDGEMENTS

The authors of this work would like to acknowledge funding for this work from the Air Force Office of Scientific Research Tasks 06SN05COR and 92SN06COR. REP and HS acknowledge AFRL contract FA871806C0076. REP acknowledges AFOSR-ASEE summer faculty fellowships at AFRL/SNHC Hanscom AFB in 2006 and 2007.

REFERENCES

1. S.J. Allen, D.C. Tsui, R. A. Logan, “Observation of the two-dimensional Plasmon in silicon inversion layers,” Phys. Rev. Lett. **38**, 980 (1977).
2. E.A. Shaner, Mark Lee, M.C. Wanke, A.D. Grine, J.L. Reno and S.J. Allen, “Single-quantum-well grating-gated terahertz Plasmon detectors,” Appl. Phys. Lett. **87**, 193507 (2005).
3. X.G. Peralta, S.J. Allen, M.C. Wanke, N.E. Harff, J.A. Simmons, M.P. Lilly, J.L. Reno, P.J. Burke and J.P.Eisenstein, “Terahertz photoconductivity and Plasmon modes in double-quantum-well field-effect transistors,” Appl. Phys. Lett, **86**, 1627 (2002).
4. P.M. Smith, S.-M. J. Liu, M.-Y. Kao, P. Ho, S.C. Wang, K.H. Duh, S.T. Fu and P.C. Chao, “W-band high efficiency InP-based power HEMT with 600 GHz f_{max},” IEEE Microwave and Guided Wave Lett. **5**, 230 (1995).

5. R. Lai, M. Barsky, T. Huang, M. Sholley, H. Wang, Y.K. Kok, D.C. Streit, T. Block, P.H. Liu, T. Gaier, and L. Samoska, "An InP HEMT MMIC LNA with 7.2-dB gain at 190 GHz," IEEE Microwave and Guided Wave Lett. **8**, 393 (1998).
6. M. Littlejohn, K. Kim, and H.Tyan, "High-field transport in InGaAs and related heterostructures", in Properties of Lattice-Matched and Strained Indium Gallium Arsenide, P. Bhattacharya, ed (No.8 in EMIS Data reviews series IEEE INSPEC, 1993).
7. L. A. Cury, J. Beerens, J. P. Praseuth, "Dependence of conduction-band effective mass on quaternary alloy composition of $(In_{0.52}Al_{0.48}As)_z(In_{0.53}Ga_{0.47}As)_{1-z}$ lattice matched to InP," Appl. Phys. Lett. **63**, 1804 (1993).
8. J.-H. Huang, T. Y. Chang, and B. Lalevic, "Measurement of the conduction-band discontinuity in pseudomorphic $In_xGa_{1-x}As/In_{0.52}Al_{0.48}As$ heterostructures," Appl. Phys. Lett. **60**, 733 (1992).
9. A. V. Muravjov, H. Saxena, R. E. Peale, C. J. Fredricksen, O. Edwards, and V. N. Shastin, "High-power terahertz p-Ge laser with injection seeding," to be published (2007).
10. L. Zheng, W. L. Schaich, and A. H. MacDonald, "Theory of two-dimensional grating couplers, Phys. Rev. B **41**, 8493 (1990).
11. C. Kittel, Introduction to Solid State Physics, 2nd Ed. (John Wiley & Sons, New York, 1956), p. 352.
12. Y. T. Dai, Y. F. Chen, and I. Lo, "Effects of band offset and nonparabolicity on the effective mass of two-dimensional electron gases in modulation-δ-doped $Ga_{0.47}In_{0.53}As$-based heterostructures," Phys. Rev. B **55**, 5235 (1997).
13. K. Hofmann, B. Spangenberg, M. Luysberg, and H. Kurz, "Properties of evaporated titanium thin films and their possible application in single electron devices," Thin Solid Films **436**, 168 (2003).